Journal of
Advances in Environmental Health Research

Summer 2022. Volume 10. Number 3

Research Paper

Evaluation of the Toxicity of Zinc Oxide Nanoparticles Upon *Staphylococcus Aureus* and *Escherichia coli* in Contaminated Water

Shadi Ashraf Nohegar[1], Arezoo Nejaei[1*], Ebrahim Fataei[2*], Mohammad Ebrahim Ramazani[2], Parvin Alizadeh Eslami[3]

1. *Department of Environmental Science and Engineering, Faculty of Agricultural and Natural Resources, Tabriz Branch, Islamic Azad University, Tabriz, Iran.*
2. *Department of Environmental Science and Engineering, Faculty of Basic Sciences, Ardabil Branch, Islamic Azad University, Ardabil, Iran.*
3. *Department of Chemistry, Faculty of Basic Sciences, Tabriz Branch, Islamic Azad University, Tabriz, Iran.*

Use your device to scan and read the article online

citation Ashraf Nohegar S, Nejaei A, Fataei E, Ramazani ME, Alizadeh Eslami P. Evaluation of the Toxicity of Zinc Oxide Nanoparticles Upon *Staphylococcus Aureus* and *Escherichia coli* in Contaminated Water. Journal of Advances in Environmental Health Research. 2022; 10(3):235-246. http://dx.doi.org/10.32598/JAEHR.10.3.1261

http://dx.doi.org/10.32598/JAEHR.10.3.1261

Article info:
Received: 22 Nov 2021
Accepted: 27 Jun 2022
Publish: 01 Jul 2022

Keywords:
Toxicity, Silver, Zinc Oxide, *Staphylococcus aureus*, *Escherichia coli*

ABSTRACT

Background: Nanoparticles (NPs) have recently attracted extensive attention in the field of elimination and reduction of microbial load in various water resources. Accordingly, this study aimed to eliminate bacterial contamination from aqueous solutions using synthesized NPs.

Methods: In the present study, zinc oxide (ZnO) and silver (Ag) ion-doped zinc oxide (Ag/ZnO, 1-6 wt%) nanoparticles were synthesized using the sol-gel process and then characterized in terms of structure, morphology, and antimicrobial activity. X-ray diffraction (XRD) was utilized to determine the nanoparticle size and crystal structure. Images from field emission-scanning electron microscopy (FE-SEM) and transmission electron microscopy (TEM) confirmed the successful production of NPs. The antimicrobial activity of ZnO and Ag1-6%/ZnO against *Staphylococcus aureus* and *Escherichia coli* was assessed by the agar well diffusion method.

Results: According to the findings, the synthesized ZnO had a hexagonal structure and the size of ZnO and Ag5%/ZnO were 32.56 nm and 12.81 nm, respectively; the field emission-scanning electron microscopy (FE-SEM) images showed that the nanoparticle sizes were 77.60 nm and 47.15 nm, respectively. Based on transmission electron microscopy (TEM) images, the mean size of ZnO and Ag5%/ZnO was 22.5 nm and 17.5 nm, respectively. The results showed that the diameter of the zone of inhibition created by Ag5%/ZnO at a concentration of 0.1 g/mL was 20 mm and 13 mm for *S. aureus* and *E. coli*, respectively.

Conclusion: The results indicated that *E. coli* was more resistant than *S. aureus*, although *E. coli* was still more resistant at low concentrations.

*** Corresponding Authors:**
Arezoo Nejaei, Assistant Professor.
Address: *Department of Environmental Science and Engineering, Faculty of Agriculture and Natural Resources, Tabriz Branch, Islamic Azad University, Tabriz, Iran.*
Phone: *+98 (912) 1853763*
E-mail: *arezoonejaei@yahoo.com*

Ebrahim Fataei, Associate Professor.
Address: *Department of Environmental Science and Engineering, Faculty of Agriculture and Natural Resources, Tabriz Branch, Islamic Azad University, Tabriz, Iran.*
Phone: *+98 (45) 33727799*
E-mail: *ebfataei@gmail.com*

1. Introduction

Accelerated development in today's world has necessitated the control of harmful microorganisms so bacterial infections have become a serious challenge these days. Pathogenic microorganisms such as *Escherichia coli* (gram-negative bacteria) and *Staphylococcus aureus* (gram-positive bacteria) are common sources of contamination, especially in swimming pools. Nanotechnology as a scientific breakthrough is a promising window to escape such problems. Nanoparticles (NPs) can kill bacteria or inhibit their growth and proliferation [1-3]. Meanwhile, zinc oxide (ZnO) NPs are a crucial photocatalyst [4] acting as an antimicrobial agent, with the ability to produce oxidizing species, which can be toxic to bacteria and show antimicrobial activity against *E. coli* and *S. aureus* [5-7]. Nano-sized metal oxides (NMOs) induce cell membrane phospholipid peroxidation and lead to bacterial inactivation. The mechanism of action of NPs is based on the generation of reactive oxygen species (ROS), radical and oxidizing species; the exposure of ROSs to bacterial membranes results in cell death [8, 9].

In the photocatalytic process on the surface of NPs, the excitation of the electrons forms an electron-hole pair. The extruded electrons due to their high reducing power can reduce the dissolved metals and oxygen, as well as the holes formed on the surface of the NPs due to their high oxidizing power can oxidize the chemical substances and water, thereby leading to the generation of ions and radicals. The result is the production of superoxide anion ($O_2^{\circ-}$), hydrogen dioxide (HO_2^-), and hydrogen peroxide (H_2O_2), as well as hydroxyl ($^\circ OH$) and hydroperoxyl (HO_2°) radicals [10-13]. The produced species can destroy the bacterial cell wall [14]. One of the main problems of using photocatalytic NPs is the rapid recombination of photo-generated electron-hole pairs [15, 16], which has been suggested to be solved by doping metal ions into the nanoparticle network. Doping metal ions with ZnO increases the antibacterial activity [17, 18]. The NPs, due to their surface charge and high surface-to-volume ratio, can inactivate microbial enzymes and DNA [19, 20], damage bacterial membranes, dissolve bacterial membrane vesicles, disperse membrane compounds, and reduce the activity of some membrane enzymes. These NPs can induce oxidative stress [21-25]. They are absorbed by nucleic acid and mitochondria, which in turn disrupt their metabolism and cause genomic mutations [26]. The NPs also bind to the outer membrane of bacteria to block the function of dehydrogenase and periplasmic enzymes, as well as inhibit DNA, RNA, and protein synthesis, thereby resulting in cell lysis [27]. A study investigated the mechanism of action via ROS production by studying the reaction between the NPs and cell membrane surface [28]. In a study, the effect of ZnO, titanium dioxide (TiO_2), and copper(II) oxide (CuO) NPs on the elimination of gram-positive and gram-negative bacteria was evaluated and it showed a direct relationship between nanoparticle concentration and the efficiency of bacterial removal [29]. Research findings showed that the ZnO NPs had strong antibacterial properties [30]. Evidence revealed that the ZnO NPs could kill 93% of *E. coli* strains [31]. In a work, the ZnO NPs could eliminate more than 90% of microbial contaminants [32].

In this study, pure ZnO NPs and Silver (Ag)-doped ZnO NPs (with different weight percent, wt%) were synthesized by the sol-gel method. Subsequently, we investigated the influence of Ag ions doped into the ZnO lattice on the structure and morphology of ZnO nanocrystals and their antibacterial effects on *S. aureus* and *E. coli*. Among the various methods, such as coprecipitation, hydrothermal, thermal hydrolysis, and dc thermal plasma, the sol-gel process is one of the best with the possibility of controlling homogeneous stoichiometry with high purity and efficiency and preparing powder with fine particle size and low cost [33]. Also, it is a very versatile process for homogeneous doping or co-doping of ions into the ZnO lattice [33]. Numerous studies have been performed to investigate the antibacterial activity of oxidized nanoparticles doped with metals such as Fe, Co, Mn, Cu, Ni, Co, Ag, Mg, Ta, Nd, Ce, La, Gd, and Sn. All these doped nanoparticles have been associated with increased antibacterial activity [6].

2. Materials and Methods

Chemicals and bacterial strains

The NPs used in this work were produced by zinc acetate dihydrate, oxalic acid dihydrate, 99.99% ethanol, and silver nitrate (as dopant). The antibacterial tests were performed using *S. aureus* (ATCC 25923), *E. coli* (ATCC 25922), and Muller-Hinton agar medium. All utilized materials were from Merck (Germany) with analytical grade.

The production method of nanoparticles

In this work, based on stoichiometric calculations, 6.585 g of zinc acetate dihydrate was dissolved in 150 cc of ethanol while magnetic stirring for 30 minutes at

300 rpm and 60°C. For the synthesis of Ag-doped ZnO NPs (1-6 wt%), according to stoichiometric calculations, the desired molar concentrations were prepared in 20 cc of ethanol at 60°C, and transferred to burette, and added dropwise to the alcoholic solution of zinc acetate. Then, 7.564 g of oxalic acid dihydrate was dissolved in 30 cc of ethanol, transferred to a burette, and added dropwise to an alcoholic solution of zinc acetate. After the oxalic acid solution was finished, the obtained solution was thoroughly stirred to complete the sol-gel reaction for 2 h at 60°C. The obtained gel was dried in an oven at 90°C for 12 h. To complete the work, the calcination was performed in a furnace at 400°C. As the calcined nanoparticles cooled inside the desiccator, the nanoparticles were pulverized inside the mortar to homogenize [33]. This action resulted in the synthesis of pure ZnO NPs. The above protocol was implemented for the synthesis of Ag-doped ZnO NPs (1-6 wt%), with the difference that before adding oxalic acid, the calculated stoichiometric values of 1 wt% to 6 wt% of silver nitrate were dissolved in 20 cc of ethanol, and added dropwise to the alcoholic solution of zinc acetate using burette; thus, AgX%/ZnO NPs (X = 1-6 wt%) were prepared.

Determination of antibacterial effects using agar well diffusion method

There are several methods to determine bacterial susceptibility to NPs; this study used the agar well diffusion method. To do this, first lawn cultures were prepared from bacterial suspension by swapping in aseptic conditions. After 10 minutes, several wells with a diameter of 5 mm and a distance of 2 cm from each other depending on the number of nanoparticle concentrations were created on the medium surface using a sterile Pasteur pipette. The bottom of the well was filled by pouring 1 mm of the liquid medium to prevent any leakage. Then, nanoparticle stocks (100 µl) were poured into wells and left for 45 minutes to be adsorbed to the medium. The media should not be shaken under any circumstances during this period. Next, the plates were incubated at 37°C for 24 h, then the results were evaluated by measuring the diameter of the zone of inhibition (ZOI). The ZOI diameters were measured by a caliper in millimeters (mm) and the mean values were calculated. The sensitivity of the tested bacteria to different concentrations of used NPs was determined.

Characterization of synthesized nanoparticles

Determination of crystal structure and particle size using X-ray powder diffraction (XRD) data

An X-ray diffractometer (XRD, PANalytical X'Pert Pro MPD; Day Petronic Company, Tehran, Iran) was used to determine the crystal structure of the synthesized NPs. The size of the crystals was estimated by calculating the angle of full width at half of the maximum peaks on the XRD spectrum. First, the strongest peak was considered at a scattering angle of 2θ, and then the peak width was obtained at half the peak intensity. The XRD patterns were measured using copper (Cu)/kα radiation with a wavelength of 0.154 nm and a setting of 40 kV and 40 mA at 2θ = 5-80°. The mean crystallite size (D, nm) was calculated using Scherrer's equation (Equation 1):

1. $D=0.89\ \lambda / (\beta \cos\theta)$

, where, D stands for the crystallite size (nm), λ for the X-ray wavelength using Cu-Kα radiation (λ=0.154 nm), β for the peak width calculated using the full width at half maximum (FWHM), and θ for the Bragg diffraction angle (in degrees) corresponding to the peak (101).

Field emission-scanning electron microscopy (FE-SEM) analysis

The FE-SEM shows the microstructure of materials by surface scanning via electron beam with much higher resolution and a much larger depth of field. The FE-SEM images of the samples were prepared by Day Petronic Company (Tehran, Iran) using an apparatus from (ZEISS, SIGMA VP-500, Germany).

Transmission electron microscopy (TEM) analysis

This method is used to determine the size and shape of NPs. Some other properties of nanomaterials, such as crystal structure, chemical composition, and morphological analysis can be obtained using electron diffraction. In this method, the electron beam is irradiated to the phosphor imaging plate by irradiating the material and passing the electron beam via the material, allowing the nanoparticles to be observed. TEM images of synthesized samples of pure and doped ZnO nanoparticles were prepared by Day Petronic Company (Tehran, Iran) using an apparatus from (Zeiss-EM10C-100KV, Germany).

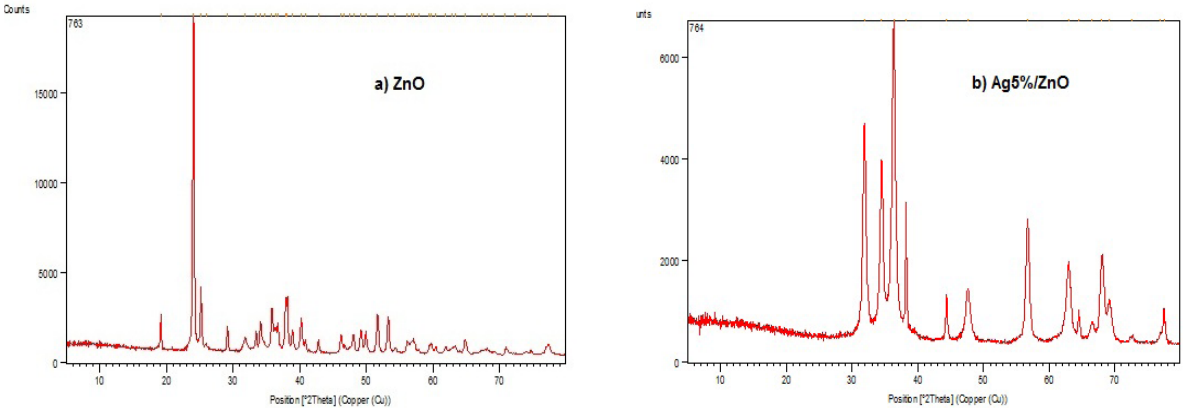

Figure 1. X-ray powder diffraction (XRD) spectra of nanoparticles synthesized Using sol-gel process
(a) Zinc Oxide (ZnO); (b) Silver (Ag) 5%/ZnO

Table 1. Mean crystallite size of synthesized nanoparticles, calculated by the debye-scherrer equation

Nanoparticles	0.89 λ	Sample β (Degree)	Modified β (Degree)	Modified β (Rad)	2θ	θ	Cos θ	βcos θ	Crystallite Size (D, nm)
ZnO	0.1371	0.256	0.246	0.0043	24.027	12.0135	0.9781	0.00421	32.56
Ag5%/ZnO	0.1371	0.66	0.65	0.0113	36.327	18.1635	0.95	0.0107	12.81

ZnO: zinc oxide; Ag: silver

3. Results and Discussion

Characterization of zinc oxide (ZnO) and silver (Ag)5%/ZnO nanoparticles (NPs) synthesized by sol-gel process

Figure 1 shows the XRD patterns of synthesized ZnO and Ag5%/ZnO NPs. These NPs were calcined at 400°C for 2 h to form a crystalline structure. The spectra with the wurtzite hexagonal crystal structure conformed well to the standard pattern of ZnO with the ID JCPDS36-1451 [34].

Based on XRD spectrum analysis, no peak of impurities, such as AgO was observed. The lack of Ag-specific diffraction in the XRD pattern of Ag-doped NPs was due to the small amount of Ag-doped element in the ZnO network or the appropriate diffusion in the ZnO network [16]. The values of 2θ for the (101) diffraction peak (the main peak of ZnO) in the XRD pattern for ZnO and Ag5%/ZnO NPs were 24.027 and 36.377 degrees, respectively. The ionic radius of Ag^{+} (1.26 Å) was larger than the ionic radius of Zn^{2+} (0.74 Å). The shift at 2θ and the broadening of diffraction peaks indicated that the dopant ions were easily and successfully introduced into the ZnO network. Due to the significant difference in the ionic radii of Ag and Zn, it was difficult to replace Ag with Zn, and Ag ions could only penetrate in the intra-network position in the ZnO network [35]. The mean crystallite size of NPs was calculated by the X-ray line broadening the (101) diffraction peak using the Debye- Scherrer equation. Table 1 presents the full results of these calculations, which clearly shows the decrease in the ZnO crystallite size due to doping.

The decrease in crystallite size was mainly due to the presence of Ag-O-ZnO on the doped ZnO surface, which inhibits the growth of crystalline particles [36]. The Ag doping also led to oxygen deficiency in the crystal structure of ZnO, resulting in the reduction of its crystallite size. The micro stress of NPs was calculated using the Equation 2:

2. $\mathcal{E}=\beta \cos\theta/4$

Table 2. Micro stress level of nanoparticles synthesized using sol-gel process

Nanoparticle Type	Nanoparticle Size (nm)	Micro Stress Level ($\varepsilon \times 10^{-3}$)
ZnO	32.56	1.1
Ag5%/ZnO	12.81	2.7

ZnO: zinc oxide; Ag: silver

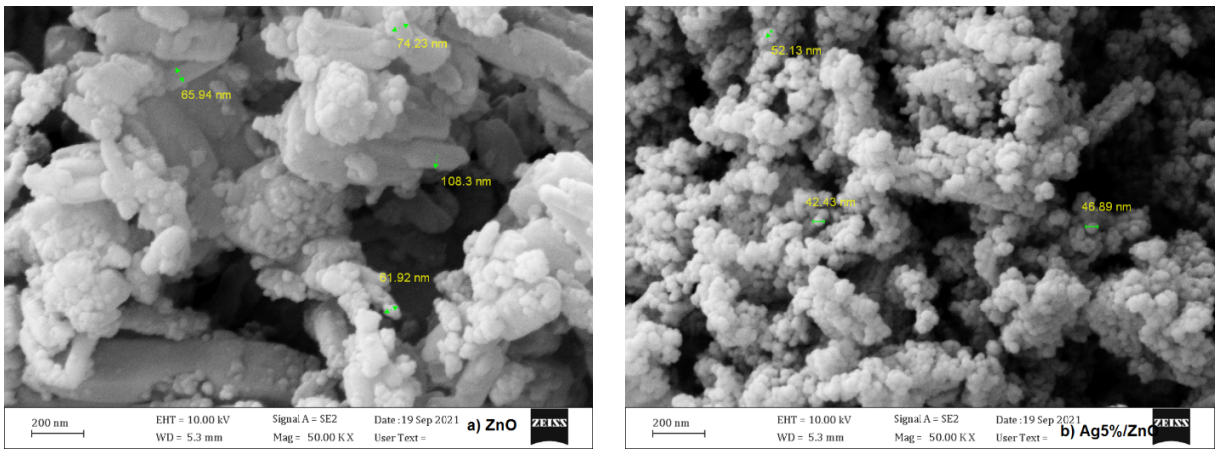

Figure 2. FE-SEM images of nanoparticles synthesized using sol-gel process
(a) Zinc Oxide (ZnO) and (b) Silver (Ag) 5%/ZnO

As shown in Table 2, the amount of micro stress was slightly changed, meaning that the increase in micro stress of NPs altered the diffraction peak broadening and decreased the particle size, resulting in less XRD peak shift. The line broadening might be related to the nanoparticle size or micro stress or the interaction between the two [37].

Morphological study of synthesized nanoparticles (NPs) using field emission-scanning electron microscopy (FESEM) and elemental analysis of nanoparticles (NPs) using energy-dispersive X-ray spectroscopy (EDX)

The FE-SEM was employed to study the structure and morphology of NPs [37]. Figure 2 shows FE-SEM images of nanoparticles synthesized using the sol-gel process. As seen in the images, the NPs have a uniform spherical morphology; the Ag doping did not affect nanoparticle morphology and also decreased the particle size. The mean size of ZnO and Ag5%/ZnO NPs was 77.60 nm and 47.15 nm, respectively. In the doped samples, the particle size was reduced. The EDX analysis was performed to investigate the chemical composition of NPs. Figure 3 shows the EDX spectrum of nanoparticles synthesized using the sol-gel process. The presence of constituent elements was visible and no peak related to impurities was observed. The EDX spectrum for pure ZnO NPs showed that the synthesized NPs contained only two elements of Zn and O, highlighting the purity of ZnO NPs. The EDX images for Ag-doped NPs also revealed that the samples were composed of Zn, Ag, and O elements, emphasizing the purity of the NPs.

Determination of nanoparticle size using transmission electron microscopy (TEM) images

Figure 4 shows the particle shape, size, and dispersion for the synthesized NPs determined by TEM images. The images displayed a slight aggregation of NPs along with dispersed particles. According to these images, all synthesized NPs had a regular dispersion and spherical morphology. The size obtained from the XRD patterns was slightly different from the TEM images because the measurement in the TEM images was done by measuring the distance between the visible particle boundaries. On the other hand, the particle size was measured on the XRD pattern in the range of the crystal region that uniformly diffracts the X-rays [38]. The size

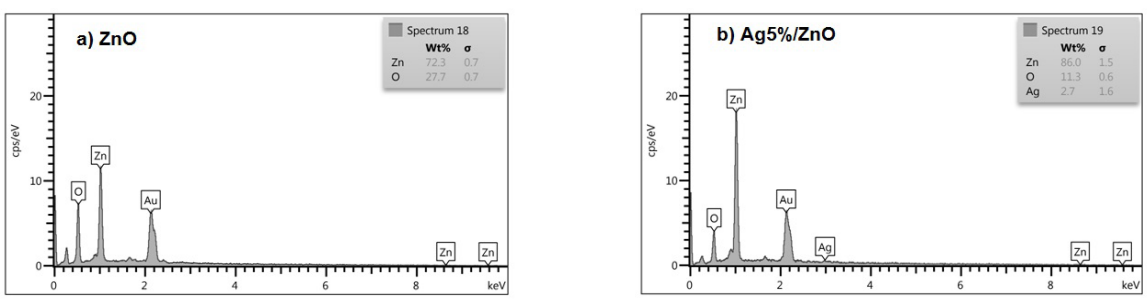

Figure 3. EDX spectra of nanoparticles synthesized using sol-gel process
(a) zinc oxide (ZnO) and (b) silver (Ag) 5%/ZnO

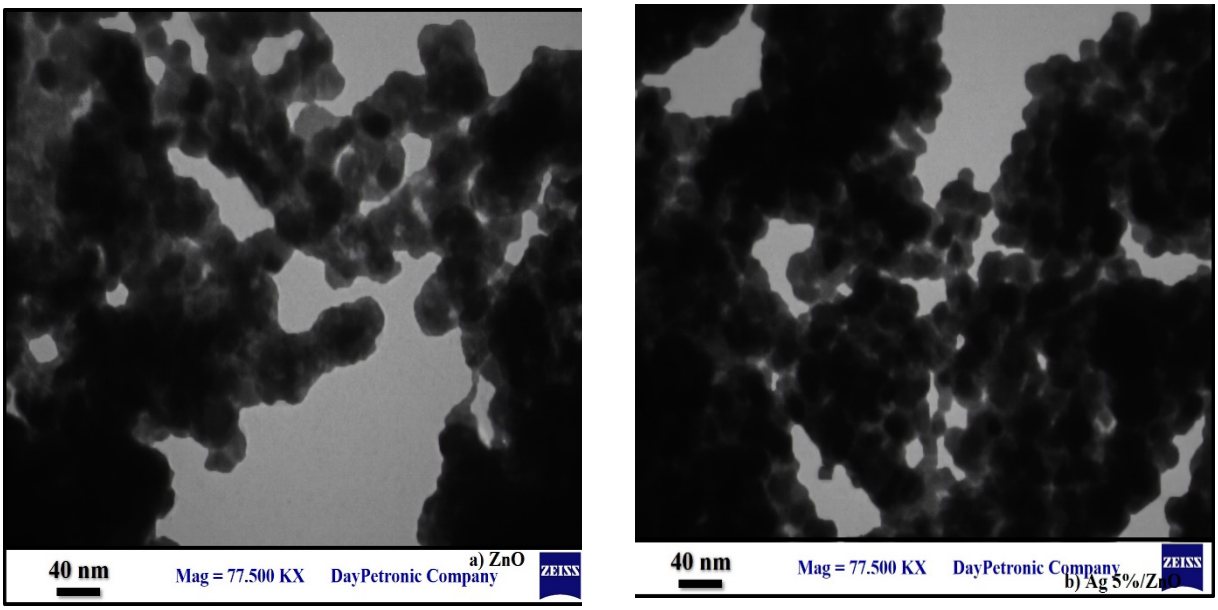

Figure 4. Transmission electron microscopy (TEM) images of nanoparticles synthesized using the sol-gel process (a) zinc oxide (ZnO) and (b) silver (Ag) 5%/ZnO

of synthesized ZnO NPs was in the range of 15 nm to 30 nm with an average of 22.5 nm and the size of synthesized Ag5%/ZnO NPs was in the range of 15 nm to 20 nm with an average of 17.5 nm. The results revealed that the particle size decreased as a result of Ag doping into the ZnO network.

Antibacterial activity of nanoparticles synthesized using the sol-gel process against bacterial strains tested

The antibacterial activity of synthesized ZnO and AgX% (X=1-6 wt%)/ ZnO NPs was determined against *S. aureus* (Figure 5a). The mean diameters of ZOI generated by the agar well diffusion method at different concentrations of NPs were calculated as shown in Table 3.

According to Table 3, the data on the mean diameter of ZOI for *S. aureus* showed that at a concentration of 0.1 g/mL of NPs, the highest diameter of ZOI (20 mm) was related to Ag5%/ZnO NPs. With decreasing the NPs concentration to 0.05, 0.025, and 0.0625 g/ml, the highest ZOI diameter was again related to Ag5%/ZnO NPs, which meant that Ag5%/ZnO NPs had the highest bacterial inhibitory activity among NPs against *S. aureus*. The antibacterial activity of synthesized ZnO and AgX% (X=1-6 wt%)/ ZnO NPs was determined against *E. coli* (Figure 5b). The mean diameters of ZOI generated by the agar well diffusion method at different concentrations of NPs were calculated as shown in Table 4.

Table 3. Mean diameter of zone of inhibition (mm) against Staphylococcus aureus at different concentrations

Concentrations and Types of NPs	0.1 g/mL	0.05 g/mL	0.025 g/mL	0.0125 g/mL	0.00625 g/mL
ZnO	13	13	12	12	11
Ag1%/ZnO	13	12	12	11	8
Ag2%/ZnO	14	12	11	11	10
Ag3%/ZnO	18	15	13	12	11
Ag4%/ZnO	13	15	14	12	11
Ag5%/ZnO	20	18	18	16	12
Ag6%/ZnO	13	12	11	11	10

ZnO: zinc oxide; Ag: silver; NPs: nanoparticles

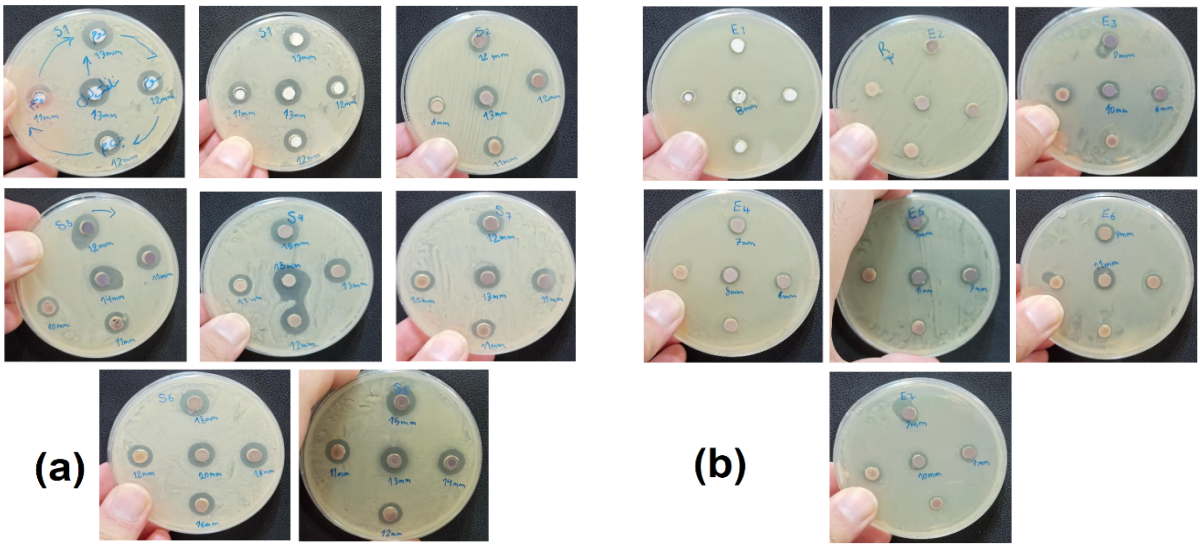

Figure 5. Antibacterial test results and zone of inhibition generated by zinc oxide (ZnO) and silver (Ag) X%/ZnO (X=1-6 wt%) nanoparticles (NPs) in the presence of (a) *S. aureus* and (b) *E. coli*

According to Table 4, the data on the mean diameter of ZOI for *E. coli* showed that, at a concentration of 0.1 g/mL of NPs, the highest diameter of ZOI (13 mm) was related to Ag5%/ZnO NPs. It had the highest bacterial inhibitory activity among NPs used against *E. coli*. The larger ZOI diameter for *S. aureus* in the presence of different concentrations of NPs indicated greater resistance of *E. coli* to these NPs compared to *S. aureus*. At lower concentrations, *E. coli* was more resistant to these NPs. By doping Ag on ZnO, the efficiency of bacterial removal increased significantly, and this doping showed the highest value at 5% by weight. The degree of cell wall vulnerability in different bacterial strains varies due to differences in membrane permeability. Therefore, the sensitivity of different bacteria was very different from each other under the same conditions, nanoparticle concentration, and contact time.

Among the synthesized NPs, Ag5%/ZnO NPs showed the highest antimicrobial activity against *S. aureus* (20 mm for 0.1 g/mL of NPs) and *E. coli* (13 mm for 0.1 g/mL of NPs). These results showed the higher resistance of *E. coli* to NPs compared to *S. aureus*, especially at lower concentrations. The mechanism of action of NPs on bacteria can be attributed to damage to proteins, DNA, and cell walls [39-41]. Due to the negative surface charge in bacteria and the positive charge in NPs, this difference between the charges acts as an electromagnetic absorber between the bacterium and the nanoparticle, so that the nanoparticle binds to the cell surface and results in cell death. Oxidation of surface molecules occurs following the attachment of NPs to the cell surface, which causes the membrane to perforate and NPs to enter the bacterial cell, thereby disrupting metabolic

Table 4. Mean diameter of zone of inhibition (mm) against Escherichia coli at different concentrations

Concentrations and Types of NPs	0.1 g/mL	0.05 g/mL	0.025 g/mL	0.0125 g/mL	0.00625 g/mL
ZnO	8	R	R	R	R
Ag1%/ZnO	R	R	R	R	R
Ag2%/ZnO	10	9	8	R	R
Ag3%/ZnO	8	7	6	R	R
Ag4%/ZnO	10	9	9	R	R
Ag5%/ZnO	13	9	R	R	R
Ag6%/ZnO	10	9	7	R	R

ZnO: zinc oxide; Ag: silver; NPs: nanoparticles

pathways and ultimately leading to the death of bacteria [42]. The possible reaction mechanism of NPs is associated with the release of ions from NPs (Zn^{2+} and Ag^{+}) that react with the functional groups of bacterial cell surface proteins, such as the thiol group. These cell membrane proteins facilitate the transport of nutrients and minerals across the wall due to their outward protrusion. By acting on these compounds, the NPs deactivate the membrane and make it impermeable to nutrients [43-45]. A study in 2007 found that the effect of Ag and Zn NPs on *E. coli* and *S. aureus* was the same, while TiO_2 NPs were more effective against *S. aureus*. The TiO_2 NPs caused loss of respiratory processes and ultimately cell death by oxidizing the membrane phospholipids of *S. aureus* and *E. coli* [44, 46, 47]. Previous studies have shown that membrane lipid compounds in *E. coli* were more resistant to NPs than in *S. aureus*. In this study, *E. coli* was more resistant as well. The ZnO NPs had antibacterial activity against gram-positive and gram-negative bacteria, and the degree of antibacterial properties depended on the susceptibility of microorganisms. The bacterial sensitivity is determined by differences in cell wall thickness. The gram-positive bacterial cell wall has a thick peptidoglycan layer, while the gram-negative bacterial cell wall has a thin peptidoglycan layer [6]. The gram-positive bacteria exposed to ZnO NPs are more affected than the gram-negative bacteria. Positively charged NPs can greatly affect gram-negative bacteria more than gram-positive bacteria. In this regard, studies have shown that gram-positive bacteria are more sensitive to Fe_2O_3, ZnO, and MgO than gram-negative bacteria. In addition, metal oxide NPs show different antibacterial properties based on their surface-to-volume ratio [48, 49]. Chung et al. concluded that the accumulation of negative charge on gram-negative bacteria was higher than on gram-positive bacteria. The interaction of positively charged NPs and negatively charged cell walls led to the leakage of bacterial intracellular contents [50]. Due to the negatively charged cell membrane, a resulting membrane electrostatic attraction directs NPs into the cell [32]. Arakha et al. investigated the antimicrobial potentials of iron oxide and copper oxide NPs against *E. coli* and Bacillus subtilis. They found that suspending NPs in the culture medium exposed them to different biological interfaces due to the existence of cell components, such as DNA, lipids, proteins, and polysaccharides. The very small dimensions of NPs due to their high surface-to-volume ratio cause a high concentration of free energy on their surfaces. Due to the electrostatic forces in biological systems, to reduce the free energy and achieve relatively high stability, these interactions with enough energy to overcome the band gap barrier of nanoparticle result in the generation of electron-hole pairs (or free electrons). The free electrons result in the formation of reactive oxygen species and subsequently induce oxidative stress. Oxidative stress is one of the vital potentials of NPs to induce toxicity, which occurs due to oxidation-reduction properties on the surface of NPs and causes inflammation in the cell leading to increased ROS production. Metal ions released from the nanoparticle surface induce ROS production. The entry of NPs into the cell results in damage to cellular components and disruption of the electron transport chain, eventually leading to ROS production [51]. Mechanisms of toxicity and antimicrobial properties reported for NPs include induction of oxidative stress via the production of ROS, release of Zn^{2+} ions and internalization of ZnO NPs via membrane binding, loss of membrane arrangement due to the membrane and intra-cellular accumulation of NPs, resulting in the destruction of bacterial cell wall and membrane by the collision of NPs with the membrane, thereby reducing cell integrity, transport interruption, inhibition of enzymatic activity and inhibition of DNA synthesis [52, 53]. The ROS production increases membrane lipid peroxidation [54], thereby degrading the unsaturated phospholipids of the bacterial cell wall and thus cell death [55-57]. In this regard, Sawai et al. investigated the role of oxygen radicals produced by ZnO in exerting an antimicrobial effect. They showed that the production of hydrogen peroxide has an antimicrobial impact, and stated that as the concentration of oxygen radicals increases, the level of hydrogen peroxide produced also increases linearly [58]. The hydrogen peroxide can pass through the cell wall and enter the bacterial cell, causing cell death. In the suspension of ZnO NPs, the partial dissolution of NPs in solution leads to the release of Zn^{2+} whose antimicrobial activity accelerates the reduction of metabolism rate and the disturbance of the enzyme system. A study investigated the antimicrobial activity of NPs based on ROS production and release of Zn^{2+} ions from ZnO NPs suspension. They found that at a concentration of 1 mg/L of Zn^{2+}, no inhibition of *E. coli* was observed; however, the growth rate of these bacteria was reduced. Studies have shown that ZnO NPs colliding with *S. aureus* causes holes in the membrane; subsequently, the ions released by transmembrane diffusion affect the DNA, thereby causing nuclear damage similar to irreparable chromosome damage [6].

Via energy absorption, ZnO NPs stimulate and activate the valence electron band and promote the electron to the conduction band, thereby creating a highly active electron-hole pair that directly or indirectly reacts with organic compounds. Electron-hole pairs

produced by migration to the interface can cause the following redox reactions [6]:

$ZnO+hv \rightarrow e^{-}+h^{+}$

$H_2O \rightarrow H^{+}+OH^{-}$

$H^{+}+OH^{-} \rightarrow HO^{\circ}$

$h^{+} + H_2O \rightarrow H^{+}+OH^{-}$

$e^{-}+O_2 \rightarrow O_2^{\circ-}$

$O_2^{\circ-}+H+ \rightarrow HO_2^{\circ}$

$2HO_2^{\circ} \rightarrow O_2^{\circ} + H_2O_2$

$H_2O_2+O_2^{\circ-} \rightarrow OH^{-}+OH^{\circ}+O_2$

$H_2O_2+hv \rightarrow 2OH^{\circ}$

Organic matters of bacterial cell wall + Radical and peroxide oxygen compounds CO_2+H_2O + inert substances

The ROS is composed of oxygen-derived free radicals, including hydroxyl radicals, superoxide anions, and highly active non-radical oxygen derivatives, such as hydrogen peroxide, peroxynitrite, and hypochlorite. The hydroxyl radicals can directly enter the photocatalytic reaction with bacteria and eventually kill them [59]. The ROS are formed in the body of organisms possessing aerobic respiration during respiratory processes or reactions of photochemical compounds in the electron transport chain in mitochondria. When the production of oxygen radicals increases, the toxic substances in the cell will increase, resulting in oxidative stress [32]. Sunada et al. investigated the mechanisms of action of TiO_2 NPs in the elimination of *E. coli*. They described the following steps for this mechanism. The outer membrane of bacteria is partially attacked and disintegrated by highly reactive species, such as OH°, $O_2^{\circ-}$, and H_2O_2. Disruption of the inner membrane arrangement leads to the membrane lipid pre-oxidation and ultimately cell destruction. The dead cells then disintegrate and *E. coli* is generally converted to carbon dioxide, water, and other minerals [60]. However, the antibacterial effects of NPs depend on their concentration (Tables 2 and 3), shape, and size [61]. According to the images, the results show that doping NPs reduces their size and consequently increases the release of nanoparticle ions from the surface and thus increases the antibacterial property [62]. By reducing nanoparticle size due to doping, NPs appear to be involved in antimicrobial mechanisms, including intrusion into the cell, interference with the membrane process, and induction of oxidative stress. However, it is emphasized that the formation of oxidative stress and free radicals is the reason for the antimicrobial effect of metal NPs [63, 64].

Aqueous suspension of ZnO accelerates the chemical interaction of hydrogen peroxide with cell membrane proteins. Due to the recombination nature of electron-hole pairs in pure NPs, to prevent recombination and increase the antimicrobial activity of NPs, researchers suggested the surface modification of NPs, which increases the dispersion and less aggregation of ZnO NPs. Doping of metal oxides is one of the crucial methods to improve the properties of NPs and prevent recombination, which leads to surface changes due to the entry of dopant ions. The presence of these impurities leads to changes in the structure of NPs and doping provides new conditions for crystal growth and severe changes in internal defects and morphology. In these defects, photocatalytic reactions are accelerated by increasing oxygen vacancy, and due to the synergistic effect of dopant ions, the production of ROS increases, and the antimicrobial activity of ZnO increases. As shown in this study, the presence of dopants alters the size of ZnO NPs [6]. One of the main reasons for using NPs over antibiotics is that NPs are not resistant to bacteria and can affect a wide range of bacteria; the NPs also influence other microorganisms after acting on the target point [65]. However, NPs such as chromium (Cr), Ag, titanium (Ti), Zn, and their oxides have shown the lowest level of toxicity in the life cycle and ecosystem due to their bactericidal properties. These nanomaterials can be suitable candidates to control pathogenic microorganisms [66].

4. Conclusion

The present study was performed on *Escherichia coli* (gram-negative bacteria) and *S. aureus* (gram-positive bacteria) due to the hazardous and pathogenic nature of these microorganisms. To control these bacteria, we successfully synthesized zinc nanoparticles (ZnO NPs) and then could dope these synthesized nanoparticles with silver ions (Ag5%/ZnO NPs) to decrease their size. The introduction of silver ions into the nanoparticle network was successful due to the difference in ionic radius and did not cause any disturbance in the morphology of the synthesized uniform spherical nanoparticles. The antimicrobial results of doped nanoparticles associated with reduced size had the highest bacterial removal efficiency. The Ag5%/ZnO NPs greatly affected *S. aureus* than *E. coli*. In practice, membrane lipid compounds in *E. coli* were more resistant to nanoparticles than in *S. aureus*. The improved positive properties of pure ZnO NPs and Ag-doped ZnO NPs suggest them as a better alternative

to control multidrug-resistant microorganisms. This is because nanoparticles act in a non-specific way and can work in paths not targeted by antibiotics.

Ethical Considerations

Compliance with ethical guidelines

There were no ethical considerations to be considered in this research.

Funding

This research was extracted from the PhD. dissertation of the Shadi Ashraf Nohegar, Department of Environmental Science and Engineering, Faculty of Agriculture and Natural Resources, Tabriz Branch, Islamic Azad University, Tabriz.

Authors' contributions

All authors equally contributed to the writing, review, and final approval of the paper.

Conflict of interest

The authors declare no conflict of interest.

Acknowledgments

The authors appreciate the esteemed president, educational and research deputies of Islamic Azad University of Tabriz for their cooperation in facilitating the implementation of this project.

References

[1] Abbaspour M, Javid AH, Jalilzadeh Yengjeh R, Hassani AH, Mostafavi PG. The biodegradation of Methyl Tert-Butyl Ether (MTBE) by indigenous Bacillus cereus strain RJ1 isolated from soil. Pet Sci Technol. 2013; 31(18):1835-41. [DOI:10.1080/10916466.2011.611562]

[2] Jalilzadeh Yengejeh R, Pourjafarian V, Afrous A, Gholami A, Maktabi P, Sharifi R. Studying Bacillus cereus's ability to biodegrade crude oil in hot areas. Pet Sci Technol. 2017; 35(3):287-91. [DOI:10.1080/10916466.2014.941068]

[3] Jalilzadeh YR, Sekhavatjou MS, Maktabi P, Arbab SN, Khadivi S, Pourjafarian V. The biodegradation of crude oil by Bacillus subtilis isolated from contaminated soil in hot weather areas. Int J Environ Res. 2014; 8(2):509-14. [**Link**]

[4] Cuevas AG, Balangcod K, Balangcod T, Jasmin A. Surface morphology, optical properties and antibacterial activity of zinc oxide films synthesized via spray pyrolysis. Procedia Eng. 2013; 68: 537-43. [DOI:10.1016/j.proeng.2013.12.218]

[5] Ghanavat Amani M, Jalilzadeh Yengejeh R. Comparison of *Escherichia coli* and Klebsiella Removal Efficiency in Aquatic Environments Using Silver and Copper Nanoparticles. J Health Sci Surveill Syst. 2021; 9(2):72-80. [Link]

[6] Lallo da Silva B, Abuçafy MP, Berbel Manaia E, Oshiro Junior JA, Chiari-Andréo BG, Pietro RCLR, et al. Relationship between structure and antimicrobial activity of zinc oxide nanoparticles: An overview. Int J Nanomedicine. 2019; 14:9395-410. [DOI:10.2147/IJN.S216204]

[7] Raghupathi KR, Koodali RTK, Manna AC. Size-dependent bacterial growth inhibition and mechanism of antibacterial activity of zinc oxide nanoparticles. Langmuir. 2011; 27(7):4020-8. [DOI:10.1021/la104825u]

[8] de Azeredo HMC. Antimicrobial activity of nanomaterials for food packaging. In: Cioffi N, Rai M, editors. Nano-antimicrobials: Progress and Prospects. New York: Springer; 2012. pp. 375-94. [DOI:10.1007/978-3-642-24428-5_13]

[9] Basith NM, Vijaya JJ, Kennedy LJ, Bououdina M, Jenefar S, Kaviyarasan V. Co-Doped ZnO nanoparticles: Structural, morphological, optical, magnetic and antibacterial studies. J Mater Sci Technol. 2014; 30(11): 1108-17. [DOI:10.1016/j.jmst.2014.07.013]

[10] Kordestani B, Yengejeh RJ, Takdastan A, Neisi AK. A new study on photocatalytic degradation of meropenem and ceftriaxone antibiotics based on sulfate radicals: Influential factors, biodegradability, mineralization approach. Microchem J. 2019; 146:286-92. [DOI:10.1016/j.microc.2019.01.013]

[11] Bayati F, Mohammadi MK, Yengejeh RJ, Babaei AA. Ag 2 O/GO/TiO_2 composite nanoparticles: Synthesis, characterization, and optical studies. J Aust Ceram Soc. 2021; 57(1):287-93. [DOI:10.1007/s41779-020-00528-3]

[12] Shokri R, Yengejeh RJ, Babaei AA, Derikvand E, Almasi A. UV activation of hydrogen peroxide for removal of azithromycin antibiotic from aqueous solution: Determination of optimum conditions by response surface methodology. Toxin Reviews. 2019; 39(3):284-91. [DOI:10.1080/15569543.2018.1517803]

[13] Karthiga V, Selvakumar S. Antibacterial activity of Zinc Oxide Ag doped Zinc Oxide Nanoparticles against *E. coli*. Chem Sci Rev Lett. 2014; 3(9):40-4. [Link]

[14] Baruah S, Pal SK, Dutta J. Nanostructured zinc oxide for water treatment. nanosci nanotechnol. Asia. 2012; 2(2):90-102. [DOI:10.2174/2210681211202020090]

[15] Zarei N, Behnajady MA. Synthesis, characterization, and photocatalytic activity of sol–gel prepared Mg/ZnO nanoparticles. Desalination Water Treat. 2016; 57(36):16855-61. [DOI:10.1080/19443994.2015.1083479]

[16] Eskandarloo H, Badiei A, Behnajady MA, Ziarani GM. Ultrasonic-assisted degradation of phenazopyridine with a combination of sm-doped ZnO nanoparticles and inorganic oxidants. Ultrason Sonochem. 2016; 28:169-77. [DOI:10.1016/j.ultsonch.2015.07.012]

[17] Ahmad M, Ahmed E, Hong ZL, Ahmed W, Elhissi A, Khalid NR. Photocatalytic, sonocatalytic and sonophotocatalytic degradation of Rhodamine B using ZnO/CNTs composites photocatalysts. Ultrason Sonochem. 2014; 21(2):761-73. [PMID]

[18] Behnajady MA, Modirshahla N, Shokri M, Zeininezhad A, Zamani HA. Enhancement photocatalytic activity of ZnO nanoparticles by silver doping with optimization of photodeposition method parameters. J Environ Sci Health A Tox Hazard Subst Environ Eng. 2009; 44(7):666-72. [PMID]

[19] Jones GL, Muller CT, O'Reilly M, Stickler DJ. Effect of triclosan on the development of bacterial biofilms by urinary tract pathogens on urinary catheters. J Antimicrob Chemother. 2006; 57(2):266-72. [PMID]

[20] Schrand AM, Rahman MF, Hussain SM, Schlager JJ, Smith DA, Syed AF. Metal-based nanoparticles and their toxicity assessment. Wiley Interdiscip Rev Nanomed Nanobiotechnol. 2010; 2(5):544-68. [PMID]

[21] Zendehdel R, Shetab-Boushehri SV, Azari MR, Hosseini V, Mohammadi H. Chemometrics models for assessment of oxidative stress risk in chrome-electroplating workers. Drug Chem Toxicol. 2015; 38(2):174-9. [PMID]

[22] Boomi P, Prabu HG, Mathiyarasu J. Synthesis and characterization of polyaniline/Ag-Pt nanocomposite for improved antibacterial activity. Colloids Surf B Biointerfaces. 2013; 103:9-14. [PMID]

[23] Perito B, Giorgetti E, Marsili P, Muniz-Miranda M. Antibacterial activity of silver nanoparticles obtained by pulsed laser ablation in pure water and in chloride solution. Beilstein J Nanotechnol. 2016; 7:465-73. [PMID]

[24] Ismail RA, Sulaiman GM, Abdulrahman SA, Marzoog TR. Antibacterial activity of magnetic iron oxide nanoparticles synthesized by laser ablation in liquid. Mater Sci Eng C Mater Biol Appl. 2015; 5:286-97. [PMID]

[25] de Azeredo HMC. Nanocomposites for food packaging applications. Food Res Int. 2009; 42(9):1240-53. [DOI:10.1016/j.foodres.2009.03.019]

[26] Singh M, Singh S, Prasad S, Gambhir IS. Nanotechnology in medicine and antibacterial effect of silver nanoparticles. Dig J Nanomater Biostructures. 2008; 3(3):115-22. [Link]

[27] King MD, Humphrey BJ, Wang YF, Kourbatova EV, Ray SM, Blumberg HM. Emergence of community-acquired methicillin-resistant *Staphylococcus aureus* USA 300 clone as the predominant cause of skin and soft-tissue infections. Ann Intern Med. 2006; 144(5):309-17. [PMID]

[28] Azam A, Ahmed AS, Oves M, Khan MS, Memic A. Size-dependent antimicrobial properties of CuO nanoparticles against Gram-positive and -negative bacterial strains. Int J Nanomedicine. 2012; 7:3527-35. [PMID]

[29] Malakootian M, Toolabi A. [Determining and comparing the effect of nanoparticle CuO, TiO_2 and ZnO in removing gram positive and negative bacteria from Wastewater (Persian)]. Toloo-e-Behdasht. 2010; 9(2-3):1-10. [Link]

[30] Nair S, Sasidharan A, Divya Rani VV, Menon D, Nair S, Manzoor K, et la. Role of size scale of ZnO nanoparticles and microparticles on toxicity toward bacteria and osteoblast cancer cells. J Mater Sci Mater Med. 2009; 20(S1):S235-41. [PMID]

[31] Raffi M, Mehrwan S, Bhatti TM, Akhter JI, Hameed A, Yawar W. Investigations into the antibacterial behavior of copper nanoparticles against *Escherichia coli*. Ann Microbiol. 2010; 60(1):75-80. [DOI:10.1007/s13213-010-0015-6]

[32] Mortimer M, Kasemets K, Kahru A. Toxicity of ZnO and CuO nanoparticles to ciliated protozoa Tetrahymena thermophile. Toxicology. 2010; 269(2-3):182-9. [PMID]

[33] Khanizadeh B, Khosravi M, Behnajady MA, Shamel A, Vahid B. Mg and La co-doped ZnO nanoparticles prepared by sol-gel method: Synthesis, characterization and photocatalytic activity. Period Polytech Chem Eng. 2020; 64(1):61-74. [DOI:10.3311/PPch.12959]

[34] Wang J, Gao L. Photoluminescence properties of nanocrystalline zno ceramics prepared by pressureless sintering and spark plasma sintering. J Am Ceram Soc. 2005; 88:1637-9. [DOI:10.1111/j.1551-2916.2005.00259.x]

[35] Shirdel B, Behnajady MA. Sol-Gel Synthesis of Ba-Doped ZnO Nanoparticles with Enhanced Photocatalytic Activity in Degrading Rhodamine B under UV-A Irradiation. Optics. 2017; 147:143-50. [DOI:10.1016/j.ijleo.2017.08.059]

[36] Anandan S, Vinu A, Mori T, Gokulakrishnan N, Srinivasu P, Murugesan V, et al. Photocatalytic degradation of 2,4,6-trichlorophenol using lanthanum doped ZnO in aqueous suspension. Catal Commun. 2007; 8(9):1377-82. [DOI:10.1016/j.catcom.2006.12.001]

[37] Gopalakrishna R, Muthukumara S. Nanostructure, optical and photoluminescence properties of Zn1-XNiXO nanoclusters by co-precipitation method. J Mater Sci: Mater Electron. 2013; 24:1069-80. [DOI:10.1007/s10854-012-0882-7]

[38] Suwanboo S. Structural and optical properties of nanocrystalline ZnO powder from Sol-Gel method. Sci Asia. 2008; 34:31-4. [DOI:10.2306/scienceasia1513-1874.2008.34.031]

[39] Belapurkar AD, Sherkhane P, Kale SP. Disinfection of drinking water using photocatalytic technique. Curr Sci. 2006; 91:73-6. [Link]

[40] Andrew M, Evan M. The nanotechnology consumer products inventory Woodrow Wilson. Paper presented at: Woodrow Wilson International Center for Scholars. 23 March 2006; Washington, DC, USA. [Link]

[41] Gurr JR, Wang AS, Chen CH, Jan KY. Ultrafine titanium dioxide particles in the absence of photoactivation can induce oxidative damage to human bronchial epithelial cells. Toxicology. 2005; 213(1-2):66-73. [PMID]

[42] Moadi T, Ghahramanzadeh R, Yosofi M, Mohammadi F. [Synthesis of silver nanoparticles using four species plant and investigation of their antimicrobial activity (Persian)]. Iran J Chem Eng. 2014; 33(4):1-9. [Link]

[43] Mehrdoost A, Jalilzadeh Yengejeh R, Mohammadi MK, Babaei AA, Haghighatzadeh A. Comparative analysis of uv-assisted removal of azithromycin and cefixime from aqueous solution using PAC/Fe/Si/Zn nanocomposite. J Health Sci Surveill Syst. 2021; 9(1):39-49. [Link]

[44] Sondi I, Salopek-Sondi B. Silver nanoparticles as antimicrobial agent: a case study on *E. coli* as a model for Gram-negative bacteria. J Colloid Inter Sci. 2004; 275(5):177-82. [PMID]

[45] Stoimenov PK, Klinger RL, Marchin GL, Klabunde KJ. Metal oxide nanoparticles as bactericidal agents. Langmuir. 2002; 18(6):6679-86. [DOI:10.1021/la0202374]

[46] Te-Hsing W, Yi-Der T, Lie-Hang S. The novel methods for preparing antibacterial fabric composites containing nano-material. Solid State Phenom. 2007; 124(4):1241-4. [DOI:10.4028/www.scientific.net/SSP.124-126.1241]

[47] Onodera Y, Iwasaki T, Chatterjee A, Ebina T, Satoh T, Suzuki T, et al. Bactericidal allophanic materials prepared from allophane soil: I. Preparation and characterization of silver/phosphorus-silver loaded allophanic specimens. Appl Clay Sci. 2001; 18(3-4):123-34. [DOI:10.1016/S0169-1317(00)00038-7]

[48] Tayel AA, El-Tras WF, Moussa S, El-Baz AF, Mahrous H, Salem MF, et al. Antibacterial action of Zinc Oxide Nanoparticles against foodborne pathogens. J Food Saf. 2011; 31(2):211-8. [DOI:10.1111/j.1745-4565.2010.00287.x]

[49] Imani S, Zagari Z, Rezaei-Zarchi S, Zand AM, Dorodiyan M, Bariabarghoyi H, et al. Antibacterial effect of CrO and CoFe2O4 nanoparticles upon *Staphylococcus aureus*. J Fasa Univ Med Sci. 2011; 1(3):175-81. [DOI:10.1186/2228-5326-2-21]

[50] Chung YC, Su YP, Chen CC, Jia G, Wang HL, Wu JG, et al. Relationship between antibacterial activity of chitosan and surface characteristics of cell wall. Acta Pharmacol Sin. 2004; 25(7):932-6. [Link]

[51] Arakha M, Pal S, Samantarrai D, Panigrahi TK, Mallick BC, Pramanik K, et al. Antimicrobial activity of iron oxide nanoparticle upon modulation of nanopar-ticlebacteria interface. Sci Rep. 2015; 5:14813. [PMID]

[52] Emamifar A, Kadivar M, Shahedi M, Soleimanian-zad S. Effect of nanocomposite packaging containing Ag and ZnO on inactivation of Lactobacillus plantarum in orange juice. Food Control. 2010; 22:408-13. [DOI:10.1016/j.foodcont.2010.09.011]

[53] Huh AJ, Kwon YJ. Nanoantibiotics: A new paradigm for treating infectious diseases using nanomaterials in the antibiotics resistant era. J Control Release. 2011; 156(2):128-45. [PMID]

[54] Tiwari V, Mishra N, Gadani K, Solanki PS, Shah NA, Tiwari M. Mechanism of Anti-bacterial Activity of Zinc Oxide Nanoparticle Against Carbapenem-Resistant Acinetobacter baumannii. Front Microbiol. 2018; 9:1218. [PMID]

[55] Fekri R, Mirbagheri SA, Fataei E, Ebrahimzadeh-Rajaei G, Taghavi L. Organic compound removal from textile wastewater by photocatalytic and sonocatalytic processes in the presence of copper oxide nanoparticles. Anthropogenic Pollution. 2021; 5(2):93-103. [Link]

[56] Sadr S, Langroudi AE, Nejaei A, Rabiee A, Mansouri N. Arsenic and Lead Removal from Water by Nano-photocatalytic Systems: A Review. Anthropogenic Pollution. 2021; 5(1):72-80. [Link]

[57] Reeves JF, Davies SJ, Dodd NJ, Jha AN. Hydroxyl radicals (*OH) are associated with titanium dioxide (TiO_2) nanoparticle-induced cytotoxicity and oxidative DNA damage in fish cells. Mutat Res. 2008; 640(1-2):113-22. [PMID]

[58] Sawai J, Kawada E, Kanou F, Igarashi H, Hashimoto A, Kokugan T, et al. Detection of active oxygen generated from ceramic powders having antibacterial activity. J Chem Eng Japan. 1996; 29(4):627-33.[DOI:10.1252/jcej.29.627]

[59] Rahmani AR, Samarghandi MR, Samadi MT, Nazemi F. Photocatalytic disinfection of coliform bacteria using UV/TiO_2. J Res Health Sci. 2009; 9(1):1-6. **[Link]**

[60] Sunada K, Watanabe T, Hashimoto K. Studies on photokilling of bacteria on TiO_2 thin film. J Photochem Photobiol. 2003; 156(1-3):227-33. [DOI:10.1016/S1010-6030(02)00434-3]

[61] Colaizzi JL, Knevel AM, Martin AN. Biophysical study of the mode of action of the tetracycline antibiotics. Inhibition of metalloflavoenzyme NADH cytochrome oxidoreductase. J Pharm Sci. 1965; 54(10):1425-36. [PMID]

[62] Suwanchawalit C, Chanhom1 P, Sriprang P, Wongnawa S. Ag-Doped TiO_2 Photocatalyst for Dye Decolorization under UV and Visible Irradiation. Paper presented at: Pure and Applied Chemistry International Conference. 5 January 2011; Bangkok, Thailand. **[Link]**

[63] Seil JT, Webster TJ. Antimicrobial applications of nanotechnology: Methods and literature. Int J Nanomedicine. 2012; 7:2767-81. [PMID]

[64] Thukkaram M, Sitaram S, Kannaiyan SK. Subbiahdoss G. Antibacterial efficacy of iron oxide nanoparticles against biofilms on different biomaterial surfaces. Int J Biomater. 2014; 2014:716080. [PMID]

[65] Gashtasbi F, Yengejeh RJ, Babaei AA. Adsorption of vancomycin antibiotic from aqueous solution using an activated carbon impregnated magnetite composite. Desalination Water Treat. 2017; 88:286-97. [DOI:10.5004/dwt.2017.21455]

[66] Mei N, Xuguang L, Jinming D, Hossheng J, Liqiao W, Bingshe Xu. Antibacterial activity of chitosan coated Ag-loaded nano-SiO2 composites. Carbohydr Polym. 2009; 78(1):54-9. [DOI:10.1016/j.carbpol.2009.04.029]